



**BVI NOISE FOR THE AH-1/OLS MODEL ROTOR IN FORWARD FLIGHT,
TAKING INTO ACCOUNT THE ROTOR STAND IN THE DNW WIND TUNNEL**

BY

**M. SCHAFFAR, J. HAERTIG and P. GNEMMI
FRENCH-GERMAN RESEARCH INSTITUTE,
SAINT-LOUIS, FRANCE**

**TWENTIETH EUROPEAN ROTORCRAFT FORUM
OCTOBER 4 - 7, 1994 AMSTERDAM**

BVI NOISE FOR THE AH-1/OLS MODEL ROTOR IN FORWARD FLIGHT, TAKING INTO ACCOUNT THE ROTOR STAND IN THE DNW WIND TUNNEL

M.Schaffar, J.Haertig, P.Gnemmi
French-German Research Institute
5 rue du Général-Cassagnou, 68301 SAINT LOUIS CEDEX (FRANCE)

Abstract

The question examined in this paper is whether the rotor stand has to be taken into account in the BVI noise calculation for the AH-1/OLS model rotor tested in the DNW wind tunnel.

To answer this question we use the rotor code ROTAR in which a body like the rotor stand can be taken into account and the ROTAC code for the noise prediction. The method is applied to a flight case of the AH-1/OLS model rotor and the results obtained are compared with the case without the stand. The test shows that the presence of the stand changes the heights of the blade/vortex interactions from + 0.2 to 0.5 chords, increases the retreating blade/wake interaction and the corresponding noise emission (+3 to 5 dB) but changes only slightly the noise emission corresponding to the advancing blade/wake interaction.

Notations

a_0	sound speed	U_∞, U_x	velocity of the ambient air
C_p	pressure coefficient	v_n	normal velocity component
C_T	thrust coefficient	x	position of the observer
C_Q	power coefficient	α_0	inclination angle of the rotor
c	chord of the blade	$\Gamma, \Gamma_{i,j}, \gamma_{i,j}^{\Gamma}$	panel-bounded circulation
D	rotor diameter	μ	advancing coefficient
(i,j)	index, chordwise and spanwise	ϕ	potential
l_r	component of the loading vector in the direction of the observer	Ψ	azimuth angle in the rotor plane
M_r	Mach number in the direction of the observer	ρ	air density
N, N_x, N_y	panel number (total, chordwise, spanwise)	τ	emission time (= $t-r/a_0$)
$p(x,t)$	acoustic pressure	θ	pitch angle
R	rotor radius	θ_0, θ_s	collective pitch cyclic pitch
r	distance between the blade element and the observer	Θ	angle of the observer in a horizontal plane (see fig.11)
t	observer time	Ω	angular rotational velocity

1.Introduction

In the past few years a great effort has been made to validate the aeroacoustic calculations with measurements [1, 5]. The tests of the AH-1/OLS model rotor in the DNW wind tunnel [6] are often used for these validations.

Nevertheless, this aeroacoustic analysis may provide the answer to the question whether the rotor stand, which looks like a top of a fuselage, has to be taken into account in the computation.

In order to answer that question, an aerodynamic code based on the Vortex Lattice Method (code ROTAR) is used and a panel method (sources and doublets) is applied as concerns the rotor stand; for the noise prediction an acoustic code (code ROTAC) based on the Ffowcs-Williams-Hawkings equation is used.

2.Description of the method

2.1.The Vortex Lattice Method

The Vortex Lattice Method is based on the Prandtl lifting surface theory (incompressible and inviscid flow). The blades are divided into panels (N_x chordwise, N_y spanwise, see figure 1), the size of the panels is smaller at the leading edge and at the tip of the blades. A bound lattice of vortex segments is used on the blade panels and the wake is built stepwise behind an emission line on which the excess of circulation at the time step n is emitted in the wake; the wake lattice is free to move at each time step at the local velocity.

With the non-penetration condition applied at each control point one obtains a system of N linear equations by applying the Biot and Savart law. The use of a vortex core growing with the age of the vortex avoids the singularity in the Biot and Savart law.

By using the Bernoulli equation the loads can be obtained for the thin rotor blades for each azimuth angle Ψ . To obtain the loads acting upon a thick blade, a local conformal mapping is used for each position in span to transform the thin blade into a thick one, assuming that the potential ϕ remains the same. With this method symmetrical profiles can be obtained by using the Joukowski transformation and unsymmetrical ones by means of the Theodersen transformation. This method was presented in detail in previous papers [1,2,3].

2.2. Rotor stand model and panelling

The rotor stand looks like a pylon and his top has a body shape which is similar to a fuselage. The characteristic lengths of the rotor stand have been provided by Dr H. Yu of the US-Army (private communication). Figure 2 shows the stand and the position of the rotor center with respect to the nose of the stand is $x/D = -0.0954$, $y/D = 0.$, $z/D = -0.106$.

This pylon is divided into planar panels (16 stations in length and 24 for each slice). On each panel there are a constant source (which is equal to the normal velocity) and a constant doublet following the method described by Maskew [7]. For each time step, the distribution of the doublets strength is obtained at the end of the time step using the influence of the rotor on the stand; these doublets serve as input for the calculation of the blade singularities for the following time step.

2.3. Noise prediction

The noise emission can now be calculated with a code which is based on the Ffowcs-Williams-Hawkings equation. The noise is computed with the complete expression of the integrals and the diffraction of acoustic waves on the stand is not taken into account in the acoustic code.

Starting from the well-known Ffowcs-Williams and Hawkings equation and following the Lowson's integration, the fluctuation of the acoustic pressure can be expressed with the following equation (when neglecting the quadrupole noise):

$$\begin{aligned}
 4 \pi \tilde{p}(\vec{x}, t) = & \int_S \left\{ \frac{\rho_0}{r(1-M_r)^2} \left[\frac{\partial v_n}{\partial \tau} + \frac{v_n}{1-M_r} \left(\frac{r_j}{r} \frac{\partial M_j}{\partial \tau} + \frac{a_0}{r} (M_r - M^2) \right) \right] d\sigma \right\}_{\tau=\tau_e} \\
 & + \int_S \left\{ \left[\frac{1}{a_0 r(1-M_r)^2} \left[\frac{r_i}{r} \frac{\partial \ell_i}{\partial \tau} + \frac{1}{1-M_r} \left(\frac{\ell_i r_i}{r} \right) \left(\frac{r_j}{r} \frac{\partial M_j}{\partial \tau} \right) \right] \right. \right. \\
 & \left. \left. + \frac{1}{r^2(1-M_r)^2} \left[\left(\frac{\ell_i r_i}{r} \right) \left(\frac{1-M^2}{1-M_r} \right) - \ell_i M_i \right] \right] d\sigma \right\}_{\tau=\tau_e}, \quad (1)
 \end{aligned}$$

where M_r , M_j , is the Mach number in the r or j direction ($j = 1$ to 3), $d\sigma$ is the

surface element, r is the distance between $d\sigma$ and the observer and r_i ($i = 1$ to 3) are the components of r , ℓ_r is the component of the loading vector $\vec{\ell}$ in the direction of the observer (which represents the load acting from the blade on the ambient fluid), ℓ_i is the i^{th} component of the loading vector, τ is the emission time ($= t - r/a_0$) at which the terms in [], have to be evaluated, a_0 is the sound speed, v_n is the scalar product between the velocity on the blade and the interior normal vector for the surface element $d\sigma$.

The first integral gives the thickness noise and the second gives the loading noise.

The noise is computed in the time domain (this is faster than a computation in the frequency domain). Our code is similar to the code WOPWOP developed by Brentner [8]. For the aerodynamic calculation the time step is 5° , whereas it is 2° or less in the acoustic calculation, the pressure coefficients being interpolated (with a linear interpolation) in the acoustic code.

3.AH-1/OLS model rotor: results with and without the stand

3.1.AH-1/OLS model rotor: the test case

One case of the AH-1/OLS model rotor tested in the DNW wind tunnel (1982, US-Army and DLR, [6]) was used for this study; this case has often been used in the literature for the validation of the acoustic codes (NASA-Ames, ONERA, ISL, DLR).

The case concerns the following parameters:

- advancing coefficient $\mu = 0.163$,
- no coning and no flapping angles,
- rotor inclination $\alpha_Q = 1^\circ$,
- collective pitch $\theta_0 = 5.31^\circ$,
- cyclic pitch $\theta_c = 1.86^\circ, \theta_s = -1.87^\circ$, with the following law:

$$\theta = \theta_0 + \theta_c \cos(\psi) + \theta_s \sin(\psi),$$
- mean thrust coefficient $C_T = 0.00535$,
- air velocity $U_\infty = 36.72$ m/s,
- temperature = 12° .

3.2. Aerodynamic results

The wake was analyzed for the isolated rotor and in the case with the stand in order to see all the possible influences of the stand. The major results will be discussed now:

- Figure 3 shows the time evolution of the computed thrust coefficient C_T ("time step" 5°) for the last computed revolution without a stand and with a stand.

The curves show roughly the same shape, but the presence of the stand enhances the retreating blade/wake interaction; the thrust is also significantly decreased for the azimuth angles Ψ between -30 and $+30^\circ$. The mean thrust obtained for the thick blade is 0.0050 for the isolated rotor and 0.0049 when the stand is taken into account.

- Figure 4 shows the contour plot of the normalized circulation in the case of the isolated rotor and in that of the rotor with the stand: the two figures have roughly the same shape, but the presence of the fuselage changes significantly the distribution near the interaction on the retreating side (interaction 1, see figure 7) and also near the interaction on the advancing side (interactions 1, 2 and 3, see fig.7). Further we can also notice that the maximum level of the circulation is reduced (nearly -20%) for the azimuth angles Ψ between -15 and $+15^\circ$; this may have the same origin as the thrust diminution for the same angles.
- Figure 5 shows two views of the wake for the same time step, one concerning the isolated rotor, one in the case of the rotor with the stand. The chosen step corresponds to the retreating blade/wake interaction: in these views we cannot notice any significant difference between the two cases.
- Figure 6 indicates the positions of all blade/wake interactions on the rotor disk for blade 1 in the case of the isolated rotor. No differences can be found when the stand is taken into account. Four interactions (1 to 4) occur with respectively the wake of blade 1, 2, 1, 2.
- Figure 7 shows the heights with respect to the rotor plane as a function of the distance r from the rotor center: figure 7a) presents the isolated rotor, figure 7b) the rotor with the stand.

Now the presence of the stand is clearly visible: all the heights of the interactions are shifted up by nearly 0.2 to 0.5 chords. The first interaction, which is situated below the rotor plane in the case of the isolated rotor, is now just above and below the blade passage when the stand is taken into account, which means a stronger interaction and stronger pressure variations on the blade; interaction 2 is also shifted up but the effect on the pressure variations will be lower; interaction 3 is now a straight line but only the inner part is shifted up by 0.3 chords; interaction 4 is practically the same in the two cases.

If we check figure 8 (which shows the age of the interactions) we can notice that the first interaction is the oldest, which means that the stand has enough time to influence the wake; interactions 3 and 4 are the youngest and they will not be influenced by the stand!

- Figure 9 presents some examples of the computed differential pressures in the case of the isolated rotor and in that of the rotor with the stand (near the leading edge and for several positions in span) as compared with the

measured differential pressures in the DNW wind tunnel. We find the same shape in all cases; the measured interactions are always found in the computation; the computed pressure level is lower than the measured one on the advancing side and almost equal on the retreating side.

When the stand is taken into account, we can notice the following points: the computed pressure level is sometimes closer to the pressures measured on the advancing side, the blade/vortex interaction peaks are a little steeper on the advancing side and much higher on the retreating side (which is also the case in the experiment).

- Figure 10 exhibits a contour plot of the difference in differential pressure near the leading edge due to the presence of the stand. On the left we find the differential pressure and on the right the time derivative of this pressure, which is strongly related to the noise emission. This figure clearly shows that the major impact of the presence of the stand is a strong increase in the derivative on the retreating side for the 300° azimuth angle and a small increase on the advancing side for the 0 to 20° azimuth angle.

3.3. Acoustics results

The loads obtained by applying the aerodynamic code are fed into the acoustic code, which does not take into account the diffraction on the fuselage. The results are described below.

- Figure 11 a) shows the horizontal noise directivities obtained for the isolated rotor in the rotor plane and below (-30° and -45°). The maximum noise emission is obtained in the forward direction in the rotor plane, which is a classical result; below the rotor plane, the maximum is obtained in the direction perpendicular to the advancing blade/wake interaction which occurs near the 50° azimuth angle.

Figure 11b) presents the directivities obtained by the difference between the case with a stand and the case without a stand for the loading noise alone: the strong effect found below the rotor plane is also obtained for the noise in the rotor plane (+ 4 to 6 dB) for azimuth angles between 40 to 90° , which is also due to the retreating BVI noise.

Figure 11 c) indicates the noise directivities obtained by the difference between the case with a stand and the case without a stand. As can be expected from figures 5 and 10, the noise emission is strongly increased (+3 to 5 dB) below the rotor plane for the lobe corresponding to the blade/wake interaction on the retreating side; at the same time the noise corresponding to the blade/wake interaction on the advancing side is only slightly changed (+-1 dB) for the plane below the rotor.

- Figure 12 a) and b) presents some noise signatures obtained 45° below the rotor plane for the two computations corresponding to the maximum noise emission of the retreating blade/wake interaction. It appears clearly that the retreating blade/wake interaction is enhanced by 4 to 5 dB if the stand is taken into account.
Figures 13 a) and b) shows the noise signatures corresponding to the maximum noise emission of the loading noise in the rotor plane for the case of the isolated rotor and in that of the rotor with a stand: the strong increase in the positive peak is obvious.
- Figure 14 a) and b) shows the noise signature computed for the positions of the microphones 2,3,7 and 9 used for experimental comparison; it can be noticed that the stand can change the noise signature qualitatively but the maximum level is nearly the same with and without a stand.

4. Conclusion

In conclusion, this paper demonstrates that the Vortex Lattice Method used with a local conformal mapping allows to compute the loads for a two-bladed rotor in advancing flight by taking into account the rotor stand.

It has also been shown that the rotor stand has an influence on the noise prediction and that influence is similar to that of a fuselage described in a previous paper [3]. For the BVI noise due to the interaction on the advancing side the stand has a weak influence; as all the testing microphones are on that side, there is probably no difficulty in validating the aeroacoustic codes! Nevertheless, for the retreating BVI there is an increase from 3 to 5 dB in the noise emission due to the rotor stand: it means that in order to obtain a complete noise directivity, the presence of the rotor stand has to be taken into account.

BIBLIOGRAPHY

- [1] M. SCHAFFAR, J. HAERTIG and P. GNEMMI
Aerodynamic loads and blade/vortex interaction noise prediction
15th European Rotorcraft Forum, Paper 3, Amsterdam, the Netherlands, 12-15 sept 1989
Also published in VERTICA, Vol. 14, No 2, 1990, pp.137-145
- [2] M. SCHAFFAR and J. HAERTIG
Computation of loads on the AH-1/OLS model rotor in forward flight and comparison with wind tunnel tests
18th European Rotorcraft Forum, Paper 17, Avignon, France, 15-17 sept 1992

- [3] M. SCHAFFAR, J. HAERTIG and P. GNEMMI
Computation of the BVI noise for the AH-1/OLS model rotor in forward flight with taking into account the fuselage.
Paper No AIAA 93-4333
15th AIAA Aeroacoustic Conference, Long Beach, CA, USA, 25-27 October 1993
- [4] Y.H. YU, Ch. TUNG, J. GALLMAN, W.R. SPLETTSTOESSER, K.J. SCHULTZ, B. van der WALL, P. SPIEGEL, G. RAHIER, B. MICHEA, M. COSTES
Aerodynamics and acoustics of rotor blade-vortex interactions: analysis capability and its validation
Paper No AIAA 93-4332
15th AIAA Aeroacoustic Conference, Long Beach, CA, USA, 25-27 October 1993
- [5] J.M. GALLMAN, Ch. TUNG, Y.H. YU, S.L. LOW
Prediction of blade-vortex interaction noise with application to higher harmonic control.
Paper No AIAA 93-4331
15th AIAA Aeroacoustic Conference, Long Beach, CA, USA, 25-27 October 1993
- [6] W.R. SPLETTSTOESSER, K.J. SCHULTZ, D.A. BOXWELL and F.H. SCHMITZ
Helicopter model rotor blade/vortex interaction noise: scalability and parametric variation.
NASA TM 86007, Dec 1984
- [7] Brian MASKEW
Prediction of subsonic aerodynamic characteristics: a case for low-order panel methods
J.Aircraft, Vol.19, No 2, February 1982, pp157-163. Also Paper 81-0252, AIAA 19th Aerospace Sciences Meeting, St.Louis, MO, USA, Jan. 12-15, 1981.
- [8] K.S. BRENTNER
Prediction of helicopter discrete frequency noise. A computer program incorporating realistic blade motions and advanced acoustic formulation.
NASA TM 87721, Oct 1986.

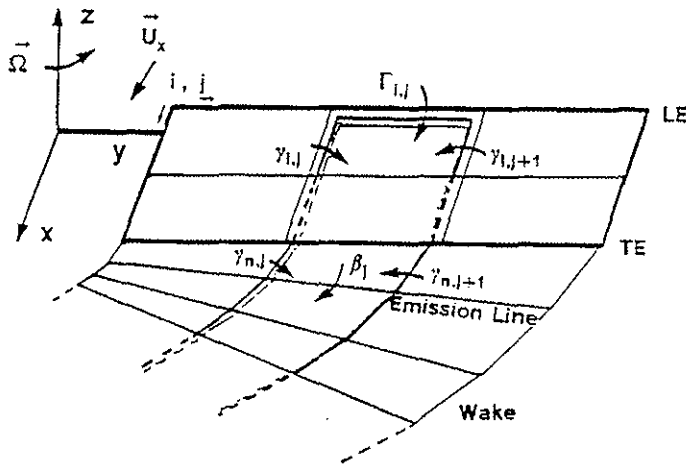


Fig. 1: Sketch of the Vortex Lattice Method.

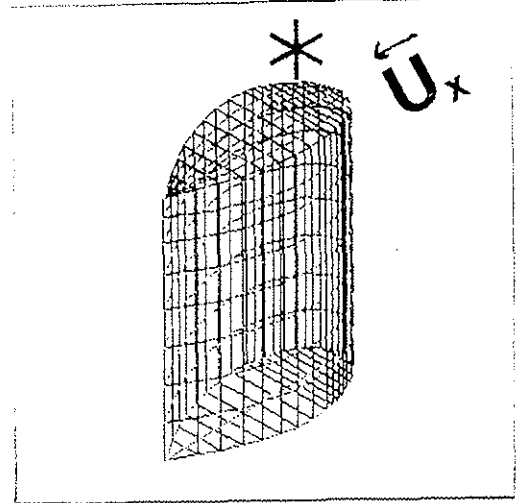


Fig. 2: Rotor stand panelling.

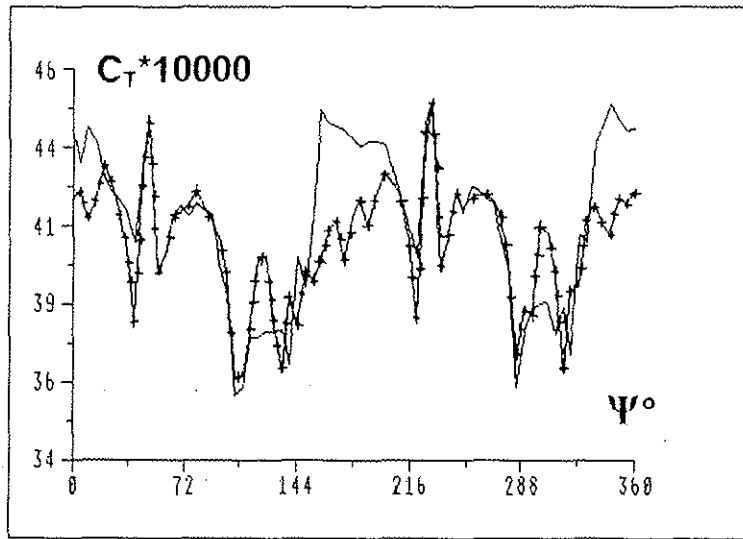


Fig. 3: Evolution of the thrust coefficient C_T :
 — = isolated rotor, +++ = rotor with a stand.

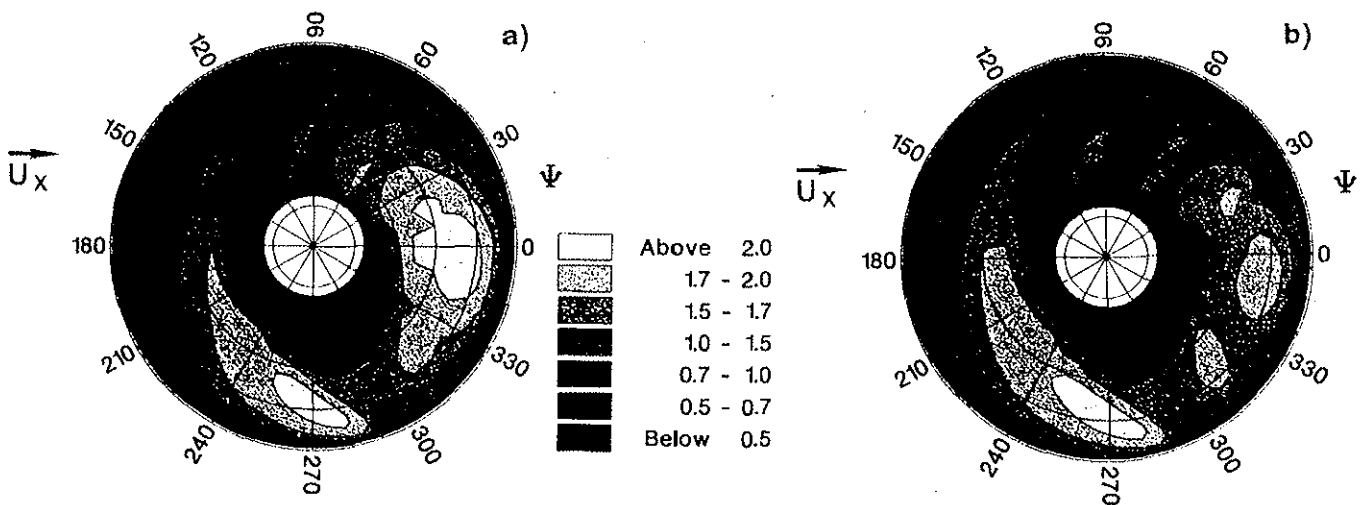


Fig. 4: Contour plot of the normalized circulation on the rotor disk:
 a) isolated rotor, b) rotor with a stand.

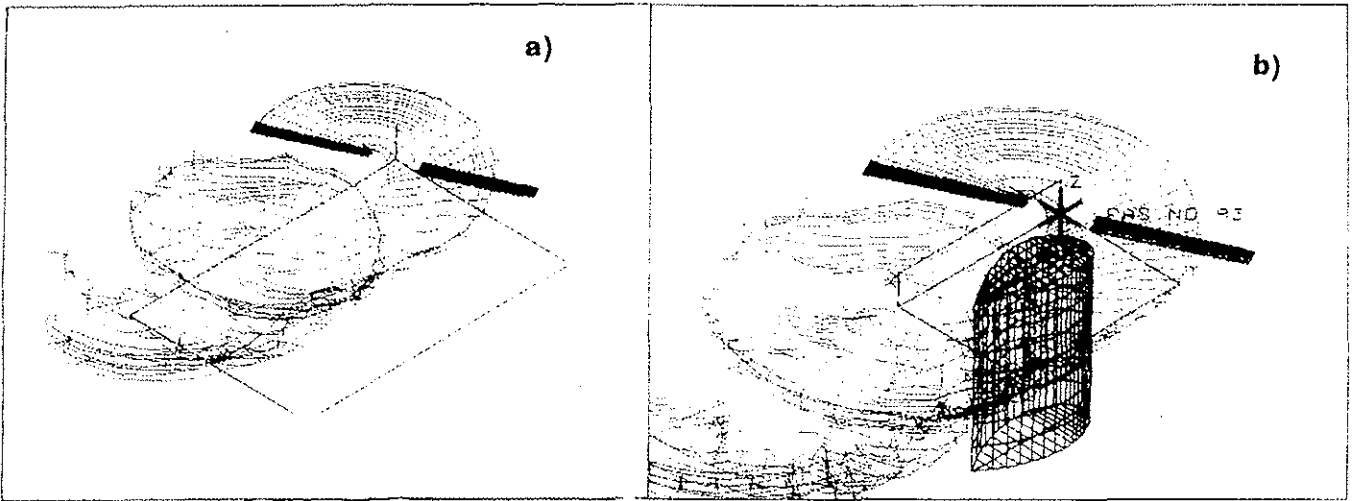


Fig. 5: View of the wake from blade 2 near the retreating BVI:
 a) isolated rotor, b) rotor with a stand.

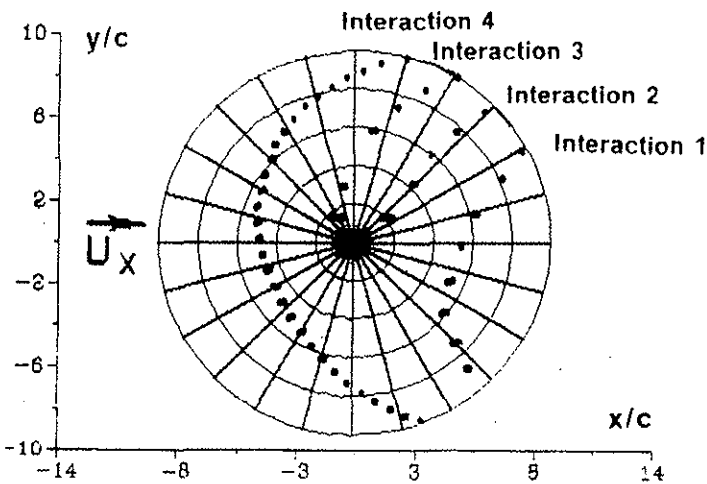


Fig. 6: Positions on the rotor disk of the blade/wake interactions for blade 1 (isolated rotor).

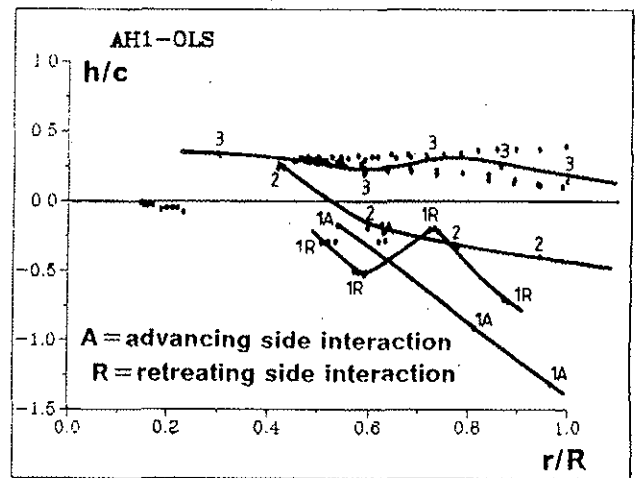


Fig. 7a: Heights of the interactions: isolated rotor.

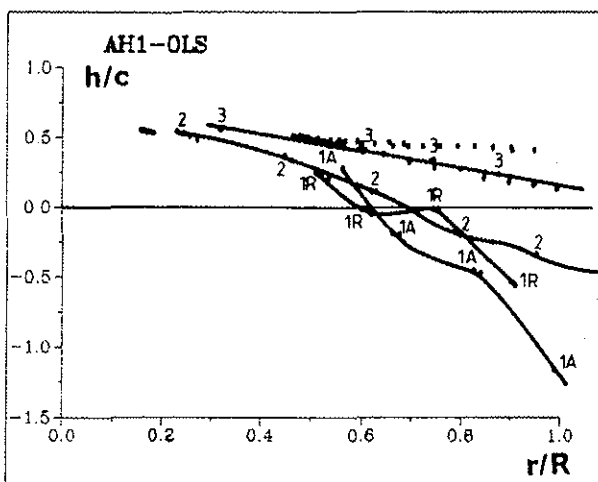


Fig. 7b: Heights of the interactions: rotor with a stand.

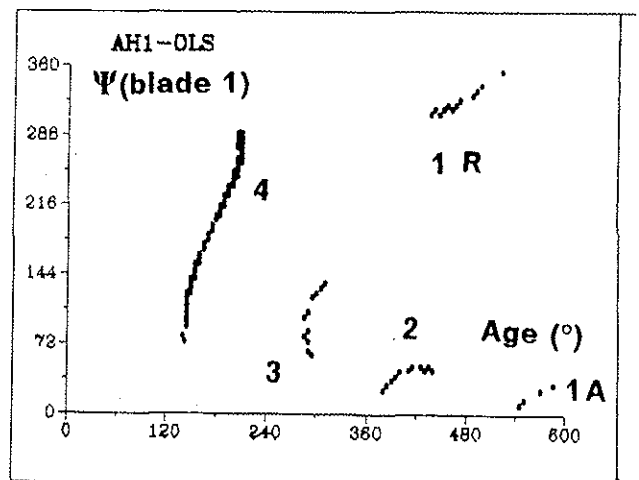


Fig. 8: Age of the interactions: rotor with a stand.

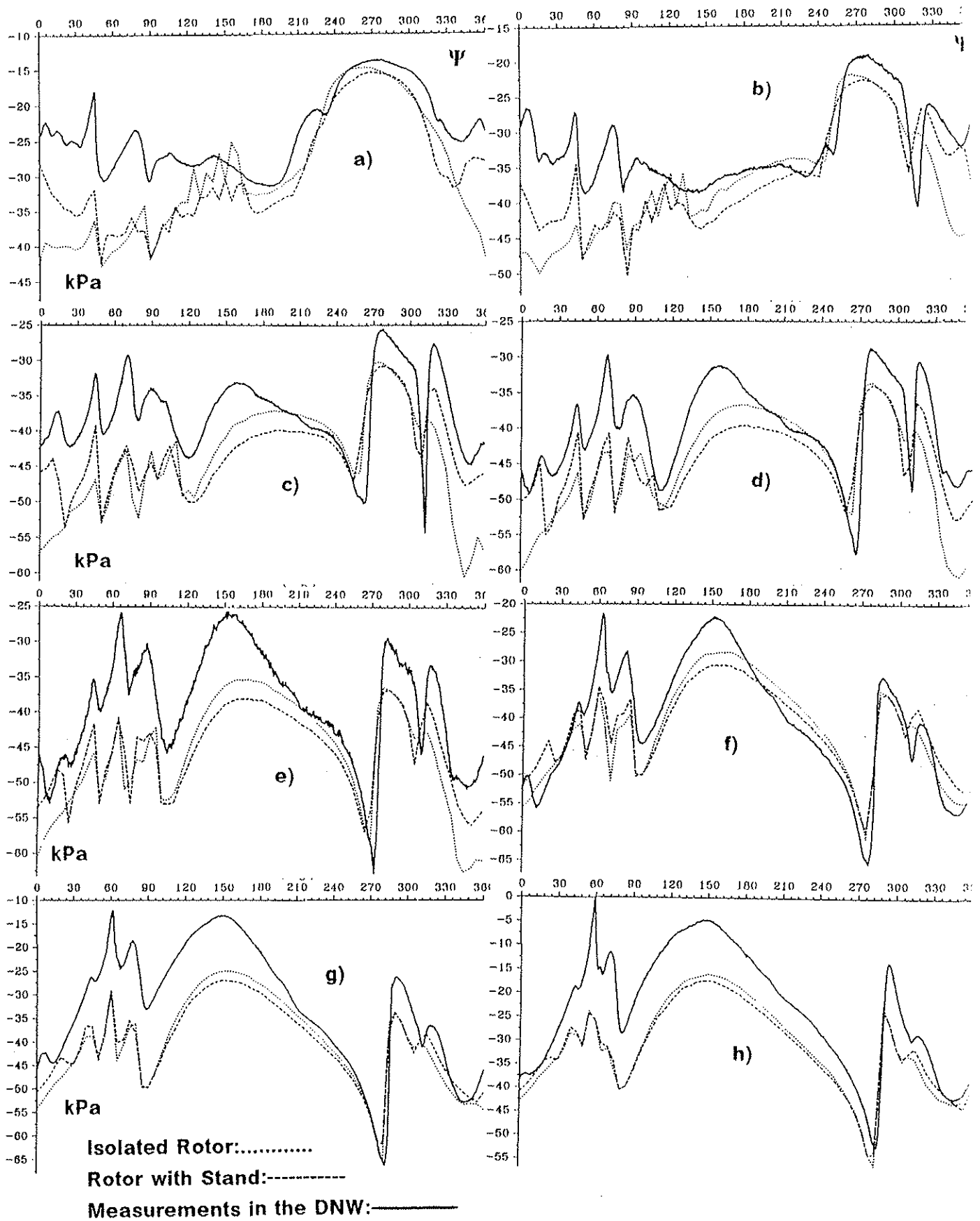


Fig. 9: Comparison of the differential pressures at $x/c=0.03$ for the measurements, the isolated rotor and the rotor with a stand; a) $y/R=0.50$, b) $y/R=0.60$, c) $y/R=0.70$, d) $y/R=0.75$, e) $y/R=0.80$, f) $y/R=0.864$, g) $y/R=0.91$, h) $y/R=0.975$.

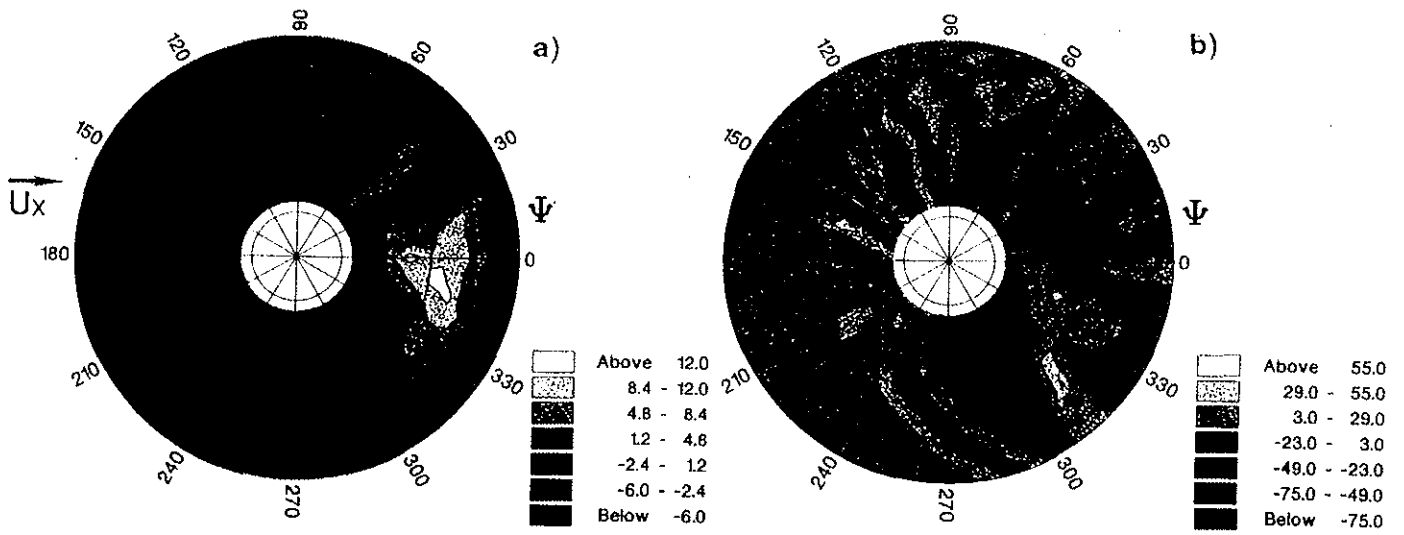


Fig. 10: Contour plot of the difference between the case rotor + stand and the case isolated rotor at $x/c=0.03$: a) pressure, b) time derivative.

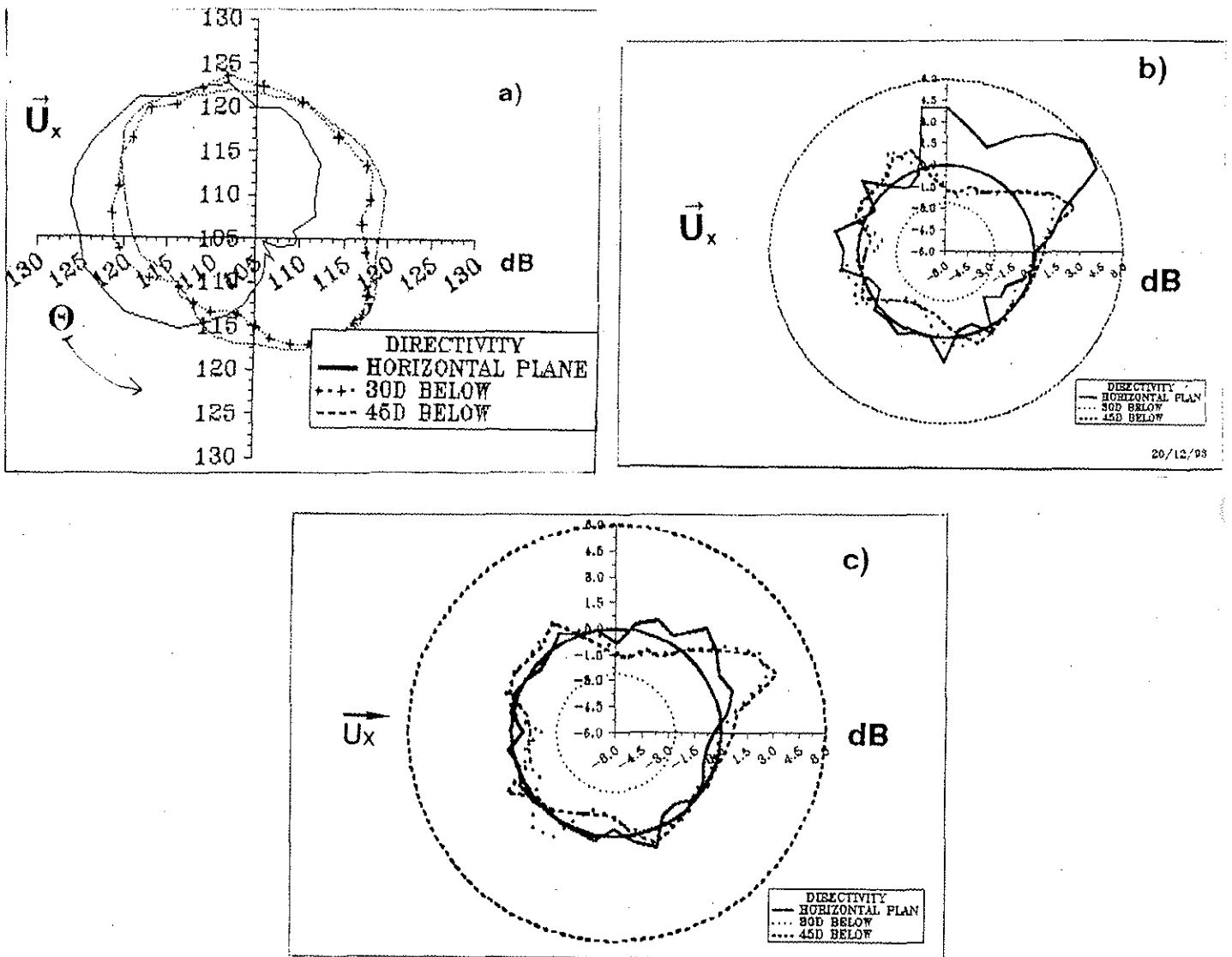


Fig. 11: Horizontal directivities: a) isolated rotor, b) ratio (dB) of the loading noise emitted by the rotor + stand and the isolated rotor, c) ratio (dB) of the total noise emitted by the rotor + stand and the isolated rotor.

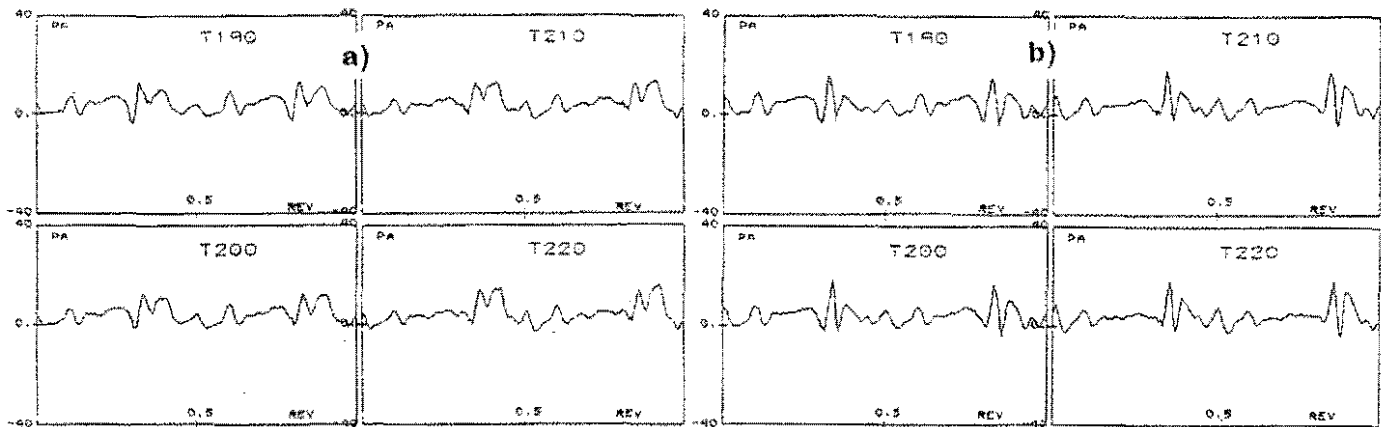


Fig. 12: Computed noise signatures 45° below the rotor plane near the maximum of the retreating BVI : a) isolated rotor, b) rotor + stand.

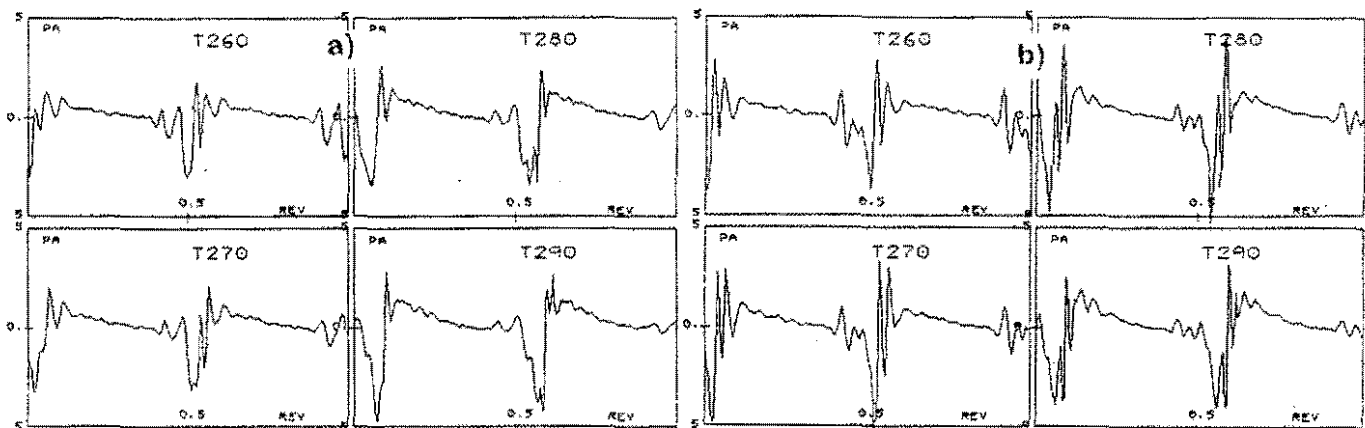


Fig. 13: Computed noise signatures of the loading noise in the rotor plane near the maximum of the retreating BVI : a) isolated rotor, b) rotor + stand.

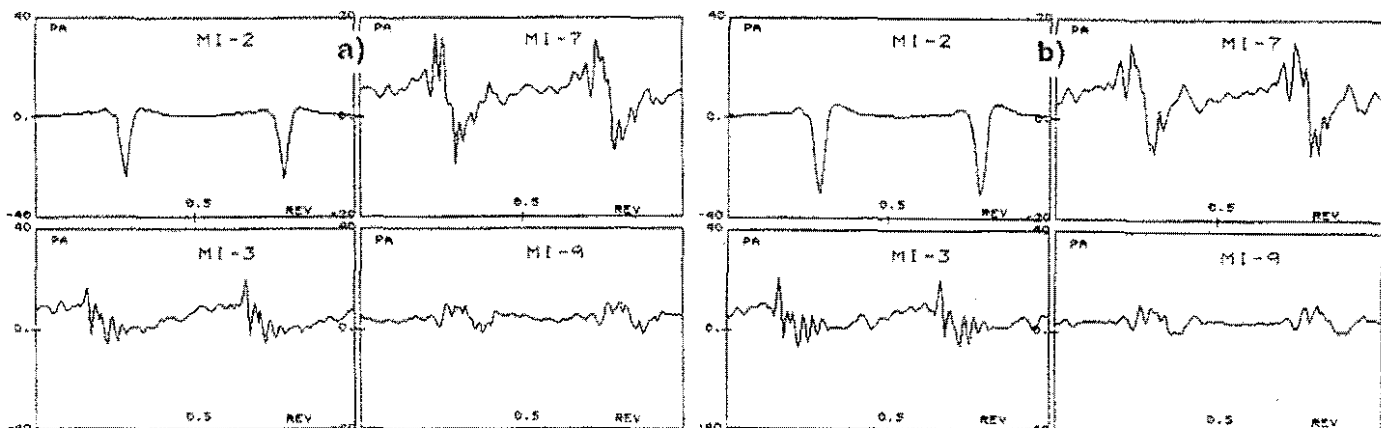


Fig. 14: Computed noise signatures for the 4 microphones 2,3,7,9 used for the validation of the aeroacoustic codes: a) isolated rotor, b) rotor + stand.